


# Identification of Positively Charged Residues in Enterovirus 71 Capsid Protein VP1 Essential for Production of Infectious Particles

Shilin Yuan,<sup>a</sup> Guiming Li,<sup>a,b</sup> Ying Wang,<sup>a</sup> Qianqian Gao,<sup>a</sup> Yizhuo Wang,<sup>a</sup> Rui Cui,<sup>a,b</sup> Ralf Altmeyer,<sup>a</sup>  Gang Zou<sup>a</sup>

Unit of Anti-Infective Research, Key Laboratory of Molecular Virology & Immunology, Institut Pasteur of Shanghai, Chinese Academy of Sciences, Shanghai, China<sup>a</sup>; School of Life Sciences, Shanghai University, Shanghai, China<sup>b</sup>

## ABSTRACT

Enterovirus 71 (EV71), a positive-stranded RNA virus, is the major cause of hand, foot, and mouth disease (HFMD) in children, which can cause severe central nervous system disease and death. The capsids of EV71 consist of 60 copies of each of four viral structural proteins (VP1 to VP4), with VP1, VP2, and VP3 exposed on the surface and VP4 arranged internally. VP1 plays a central role in particle assembly and cell entry. To gain insight into the role of positively charged residues in VP1 function in these processes, a charged-to-alanine scanning analysis was performed using an infectious cDNA clone of EV71. Twenty-seven mutants containing single charged-to-alanine changes were tested. Sixteen of them were not viable, seven mutants were replication defective, and the remaining four mutants were replication competent. By selecting revertants, second-site mutations which could at least partially restore viral infectivity were identified within VP1 for four defective mutations and two lethal mutations. The resulting residue pairs represent a network of intra- and intermolecular interactions of the VP1 protein which could serve as a potential novel drug target. Interestingly, mutation K215A in the VP1 GH loop led to a significant increase in thermal stability, demonstrating that conditional thermostable mutants can be generated by altering the charge characteristics of VP1. Moreover, all mutants were sensitive to the EV71 entry inhibitor suramin, which binds to the virus particle via the negatively charged naphthalenetrisulfonic acid group, suggesting that single charged-to-alanine mutation is not sufficient for suramin resistance. Taken together, these data highlight the importance of positively charged residues in VP1 for production of infectious particles.

## IMPORTANCE

Infection with EV71 is more often associated with neurological complications in children and is responsible for the majority of fatalities. No licensed vaccines or antiviral therapies are currently available for the prevention or treatment of EV71 infection. Understanding the determinants of virion assembly and entry will facilitate vaccine development and drug discovery. Here, we identified 23 out of 27 positively charged residues in VP1 which impaired or blocked the production of infectious particles. The defect could be rescued by second-site mutations within the VP1 protein. Our findings highlight the importance of positively charged residues in VP1 during infectious particle production and reveal a potential strategy for blocking EV71 infections by inhibiting intra- or intermolecular interactions of the VP1 protein.

Enterovirus 71 (EV71) is a nonenveloped icosahedral RNA virus belonging to genus *Enterovirus* within the family *Picornaviridae*. Since its first isolation from the stool of an infant with encephalitis in California in 1969 (1), EV71 has been recognized as a major cause of hand, foot, and mouth disease (HFMD), which is associated with severe neurological symptoms in a small proportion of cases (2). There has been a significant increase in EV71 epidemic activity throughout the Asia-Pacific region since 1997 (3–7). No approved antiviral therapeutics are currently available for clinical treatment of EV71 infections, and approval is still pending for three EV71 vaccine candidates which completed phase III clinical trials in 2013 (8). Understanding the molecular mechanism of viral replication is essential for the prevention and treatment of EV71 infections.

The genome of EV71 is a single-stranded, positive-sense RNA of approximately 7.5 kb or nucleotides (nt) in length, with a 22-amino-acid (aa) virus-encoded protein (VPg) covalently linked to the 5' end and polyadenylated at its 3' end. Flanked by 5' and 3' untranslated regions (NTRs), the single open reading frame (ORF) encodes a large polyprotein, which is processed by viral proteases into four structural proteins (VP4, VP2, VP3, and VP1) and seven nonstructural proteins (2A, 2B, 2C, 3A, 3B [VPg], 3C,

and 3D) (9). The structural proteins are involved in viral particle formation, and the nonstructural proteins are mainly responsible for viral RNA replication (10).

The capsid of EV71 consists of 60 copies of structural subunits, which are comprised of four structural proteins, VP1 to VP4. During assembly, proteolytic processing of the viral polyprotein results in the cleavage of P1 into VP0, VP1, and VP3. These proteins assemble into protomers, five of which join together to form a pentamer and 12 of which then self-assemble into the icosahedral provirion in association with a copy of the viral RNA genome (11);

Received 28 September 2015 Accepted 17 October 2015

Accepted manuscript posted online 28 October 2015

Citation Yuan S, Li G, Wang Y, Gao Q, Wang Y, Cui R, Altmeyer R, Zou G. 2016. Identification of positively charged residues in enterovirus 71 capsid protein VP1 essential for production of infectious particles. *J Virol* 90:741–752. doi:10.1128/JVI.02482-15.

Editor: R. M. Sandri-Goldin

Address correspondence to Ralf Altmeyer, raltmeyer@ips.ac.cn, or Gang Zou, gangzou@ips.ac.cn.

Copyright © 2015, American Society for Microbiology. All Rights Reserved.

VP0 is further processed into VP2 and VP4 in a reaction that is autocatalyzed by viral RNA and results in formation of the mature viral capsid (12, 13). In the mature capsid, VP1 to -3 together form the icosahedral shell of the virion (pseudo- $T = 3$ ), while VP4 is distributed on the inner surface of the particle (14, 15). Upon binding to a cellular receptor(s), such as P-selectin glycoprotein ligand 1 (PSGL-1) (16), scavenger receptor B2 (SCARB2) (17), sialylated glycans (18, 19), annexin II (20), heparin sulfate (21), or vimentin (22), the EV71 virions undergo an important conformational change to convert into an expanded, altered “A-particle.” The A-particle lacks the internal capsid protein VP4 and exposes N-terminal amphipathic sequences of VP1, allowing for its direct interaction with a lipid bilayer. The genomic RNA then exits via a 2-fold channel near the icosahedral 2-fold axis of symmetry and passes through a pore in the endosomal membrane into the cytosol, leaving behind an empty capsid shell (23).

Among the capsid proteins of EV71, VP1 is the most external, surface accessible, and immunogenic structural protein. Several key residues in the VP1 protein involved in pathogenesis have been identified. A nonconservative amino acid change in VP1 located within the BC loop (L97R) contributes to dissemination and neurotropism in immunocompromised patients (24). The residue at position 145 of VP1 (VP1-145) controls virus tropism by changing the accessibility of the positively charged lysine side chain of VP1-244 to the negatively charged N terminus of PSGL-1 on leukocytes (25) and has been implicated as one of the possible determinants of virulence in humans (26, 27). Moreover, VP1 is an attractive target for identification of EV71 inhibitors. BPR0Z-194, one of the pyridyl imidazolidinones developed based on WIN compound templates, is a selective EV71 inhibitor that targets VP1, and the VP1 V192M single mutation can confer resistance to the inhibitory effects (28). The suramin analog NF449 blocks EV71 infection at the step of virus binding, and NF449-resistant viruses contain double mutations (E98Q and K244R) in the VP1 protein (29).

To further understand the role of VP1 in formation of infectious particles, we performed charged-to-alanine scanning of this protein. We identified 23 out of 27 positively charged residues in VP1 to be critical for infectious particle production. Further analyses identified compensatory second-site mutations within VP1. Moreover, mutant K215A displayed a higher thermal stability phenotype, and all mutants were sensitive to suramin, which was recently identified as an entry inhibitor of EV71 (30, 31). Strategies to target these residues with inhibitors that inhibit these interactions would be predicted to impair infectious particle production, thereby limiting virus infection.

## MATERIALS AND METHODS

**Cells, viruses, and antibodies.** African green monkey kidney cells (Vero) were propagated and maintained in Dulbecco’s modified Eagle’s medium (DMEM) supplemented with 10% fetal bovine serum (FBS) and 100 U/ml of penicillin-streptomycin in a humidified incubator with 5% CO<sub>2</sub> at 37°C (Thermo Scientific). EV71 strain G082 (genotype C4) was derived from an infectious cDNA clone (32). Anti-EV71 monoclonal antibody MAB979 was purchased from Merck Millipore, Alexa Fluor 488-conjugated goat anti-mouse IgG was purchased from Life Technologies, and horseradish peroxidase (HRP)-conjugated goat anti-mouse IgG heavy- and light-chain antibody was purchased from Bethyl Laboratories, Inc.

**Plasmid construction.** Specific mutations in the VP1 region were constructed with an infectious cDNA clone of EV71 (designated pFLEV71) (32) using a Fast site-directed mutagenesis kit (TransGen Bio-

tech) according to the manufacturer’s instructions. The sequences of primers used for mutagenesis are available upon request. The DNA fragment containing the desired mutation was cut and pasted back into the original pFLEV71 at SphI and ClaI sites (nucleoside position 2252 and 4161 of the viral genome, respectively). All constructs were verified by DNA sequencing.

**In vitro transcription, RNA transfection, and IFA.** The genome-length RNA of EV71 was transcribed *in vitro* from the corresponding cDNA plasmids that were linearized with NotI. A MEGAscript T7 kit (Ambion) was used for RNA synthesis according to the instructions of the manufacturer. The RNA transcripts were dissolved in RNase-free water and stored at -80°C in aliquots. For each transfection, 10 µg of RNA was electroporated into  $8 \times 10^6$  Vero cells in 0.8 ml of cold phosphate-buffered saline (PBS) (pH 7.5) in a 0.4-cm cuvette with the GenePulser apparatus (Bio-Rad) at settings of 0.45 kV and 25 µF, pulsing three times at 3-s intervals. After a 10-min recovery at room temperature, the transfected cells were resuspended in 15 ml of prewarmed medium, and 500 µl of cell suspension was seeded into each well of 8-well culture slides (BD Falcon) for immunofluorescence assay (IFA). The remaining cells were incubated in a T-75 flask at 37°C with 5% CO<sub>2</sub>. The viruses in the culture fluids were collected at 24, 48, and 72 h posttransfection (p.t.). Aliquots of the viruses were stored at -80°C.

For the IFA, at 48 h p.t., Vero cells transfected with genome-length RNA were fixed in cold methanol at 4°C for 30 min. The fixed cells were washed twice with PBS with 0.05% Tween 20 (PBS-T) and incubated with anti-EV71 monoclonal antibody at room temperature for 1 h, followed by three washings with PBS and incubation with Alexa Fluor 488-conjugated goat anti-mouse IgG at room temperature for 1 h. After three washings with PBS and mounting with DAPI (4',6'-diamidino-2-phenylindole), the slides were visualized under a fluorescence microscope (Leica Microsystems). Cell images were taken at a magnification of  $\times 200$ .

**Plaque assay and infectious center assay.** Virus titers and plaque morphologies were determined by plaque assay as described previously (32). For all mutants which did not produce plaques by plaque assay, we performed an immunostaining-based infectious center assay to visualize the production of infectious noncytopathic virus (33). Briefly, approximately  $3 \times 10^5$  Vero cells per well were seeded in a 12-well plate (Corning Costar) 24 h in advance. A series of 1:10 dilutions were made by mixing 25 µl of virus sample with 225 µl of DMEM containing 2% FBS and 100 U/ml of penicillin-streptomycin. Two hundred microliters of 10-fold dilutions of viral supernatant was seeded to individual wells of 12-well plates. The plates were incubated at 37°C with 5% CO<sub>2</sub> for 1 h with shaking every 15 min, and then the virus inocula were replaced with 1 ml of DMEM plus 0.8% methylcellulose (Aquadice II; Calbiochem) and 2% FBS. After 6 days of incubation at 37°C with 5% CO<sub>2</sub>, the methylcellulose layer was peeled off, and the cells were fixed in 4% paraformaldehyde (PFA) for at least 20 min at room temperature, incubated with 0.25% Triton X-100 in PBS for 20 min, washed twice with PBS, and incubated with 200 µl of 1:1,000-diluted mouse anti-EV71 monoclonal antibody for 1 h at room temperature. The cells then were washed three times with PBS-T, incubated with 200 µl of 1:6000-diluted HRP-conjugated goat anti-mouse IgG for 1 h at room temperature, and washed three times with PBS-T, and color was developed by using a TrueBlue peroxidase substrate kit (KPL) according to the manufacturer’s instructions.

**Selection and sequencing of revertant viruses.** Mutant viruses defective in production of infectious virus particles were subjected to revertant analysis by continuously culturing on Vero cells up to 20 rounds. For each round of culturing, Vero cells ( $1 \times 10^6$  cells) in a T-25 flask were infected with 500 µl of culture supernatant derived from the previous passaging and cultured in DMEM with 2% FBS in 5% CO<sub>2</sub> at 37°C. The cytopathic effect (CPE) was monitored daily under a microscope. The incubation period was 5 days unless an apparent cytopathic effect appeared earlier. Viral RNA was extracted from culture supernatants using a QIAamp viral RNA minikit and then subjected to reverse transcription-PCR (RT-PCR) using the SuperScript III one-step RT-PCR kit (Invitrogen). The gel-pu-

rified RT-PCR products were subjected to DNA sequencing for the entire VP1 region or whole genome.

**Growth curves.** Vero cells were seeded at  $3 \times 10^5$  cells per well in 12-well plates. After incubation overnight, the cells were inoculated with either the wild-type (WT) or recombinant EV71 at a multiplicity of infection (MOI) of 0.1 in duplicate wells. The inocula were removed after 1 h of adsorption at 37°C, the monolayers were washed three times with medium, and 1 ml of medium containing 2% FBS was then added to each well. The medium was sampled every 24 h until 120 h postinfection (p.i.), and the aliquots were stored at  $-80^\circ\text{C}$  prior to titration. Virus titers in each sample were determined by plaque assay as described above.

**Thermal inactivation assays.** Virus suspensions were diluted in culture medium supplemented with 2% FBS to a concentration of about 10,000 PFU/ml. Aliquots (100  $\mu\text{l}$ ) in thin-walled PCR tubes were incubated at a constant temperature (42°C) for different amounts of time, and the titer of the remaining virus in each tube was determined by plaque assay as described above. Wild-type virus was used in each heat inactivation experiment as a positive control to normalize the results.

**CPE assay.** CPE assay was performed as described previously (32) to test the sensitivity of mutant viruses to suramin. Briefly, Vero cells (5,000 cells in 50  $\mu\text{l}$  of DMEM) were seeded into each well of a white 96-well plate (Corning Costar) and incubated at 37°C with 5%  $\text{CO}_2$  for 24 h prior to infection. Five microliters of 2-fold serial dilutions of suramin was added to the plates. Within 10 min of compound addition, 45  $\mu\text{l}$  of diluted virus (125 PFU, which corresponds to an MOI of 0.025 based on an initial cell plating density of 5,000 cells/well) was added to each well. In cell control wells, 45  $\mu\text{l}$  of assay medium was added. The final assay volume was 100  $\mu\text{l}$ /well. Plates were incubated at 37°C for 96 h and then allowed to equilibrate to room temperature for 30 min. Afterward, 50  $\mu\text{l}$  of CellTiter-Glo (Promega) reagent was added to each plate well, and the plates were incubated at room temperature for 10 to 30 min before being read with a Veritas microplate luminometer (Turner BioSystems).

## RESULTS

### Structure and sequence analyses of EV71 capsid protein VP1.

EV71 can be phylogenetically classified into 3 main genogroups (A, B, and C) and 11 genotypes (A, B1 to B5 and C1 to C5) based on VP1 sequences (34). To analyze the positively charged residues in EV71 VP1, an amino acid sequence alignment among all the genotypes of EV71 was conducted. As shown in Fig. 1, the alignment revealed a series of highly conserved amino acids across the entire region of VP1. There are 11 lysine and 16 arginine residues in the VP1 region of our EV71 G082 strain (genotype C4), and 24 of them are completely conserved among all genotypes. Residues R18 and K242 are conserved among subgenogroups B and C, whereas subgenogroup A encoded K18 and Q242, respectively. Residue K43 is conserved among subgenogroups A and C but distinct in subgenogroup B, which encodes E at this position. Structure analysis of EV71 VP1 showed that residues R120, R121, and K122 are located in  $\alpha$ -helix 3, residue R130 is located in  $\beta_{\text{D}}$ , residue K182 is located in  $\beta_{\text{E}}$ , residue R236 is located in  $\beta_{\text{H}}$ , residues R250, R254, K256, and R259 are located in  $\beta_{\text{I}}$ , and the remaining residues are located in the N and C termini or loops (summarized in Table 1) (14, 35). In the crystal structure of EV71, residues R120, R121, R122, R130, R254, K256, R264, and R267 were buried inside the capsid, and the remaining residues were exposed on the surface.

**Phenotypic characterization of charged-to-alanine scanning EV71 VP1 mutants.** To analyze the role of positively charged residues in VP1, charged-to-alanine scanning was used to create a panel of EV71 VP1 mutants. After the transfection of Vero cells with equal amounts of *in vitro*-transcribed genome-length RNAs, the percentages of IFA-positive cells, virus production, and plaque

morphology were compared between the wild type (WT) and the mutants. IFAs showed that similar percentages of IFA-positive cells were detected for the WT and mutants R18A, K162A, K218A, and K285A, whereas the percentage of IFA-positive cells was obviously reduced for mutants R3A, R38A, K43A, and R86A and IFA was negative for the remaining mutants (Fig. 2A and Table 1). In parallel, culture supernatants from transfected cells were quantified by plaque assay at each time point posttransfection to analyze production of infectious virus. Four out of the 27 mutants (R18A, K162A, K218A, and K285A) produced amounts of infectious viruses similar to that for the WT with no significant difference in plaque morphology, five mutants (R3A, R38A, K43A, R86A, and K215A) produced smaller amounts of infectious viruses than the WT with smaller plaque size, and mutants K242A and K244A were detected by infectious center assay, while the remaining mutants did not produce plaques in either the plaque assay or the infectious center assay (Fig. 2A and B). Sequencing of the complete VP1 gene of the 11 mutant viruses which are capable of producing infectious virus confirmed that only the engineered mutations were retained. It should be noted that the results of plaque assay are consistent with those of IFA for all the mutants except mutant K215A, which yielded infectious viruses at 72 h p.t. but was IFA negative at 48 h p.t., suggesting that the K215A mutation delayed virus particle production. Overall, these data suggest that most of the positively charged residues in VP1 are important for infectious particle production, except residues R18, K162, K218, and K285.

**Revertant analysis of mutants.** The identification of second-site mutations that restore the infectivity of charged-to-alanine mutants could reveal potential interacting partners of VP1 required for production of infectious particles. Therefore, seven defective and 16 lethal mutants were subjected to revertant analysis by continuous passaging of culture supernatants on Vero cells up to 20 rounds. Cytopathic effect (CPE), an indication of the presence of infectious virus, was monitored daily under a microscope for each passage. Mutants R3A, R38A, K43A, R86A, R120A, K215A, and K242A displayed obvious CPE before 5 rounds of passage (P5); mutants K244A, R250A, and K274A displayed CPE later than P5; and no plaque-forming variant could be obtained for the remaining mutants even by P20 (Table 1). Sequencing of the VP1 region of recovered viruses revealed a reversion to the WT sequence for mutants K43A (mixed in sequencing chromatogram), R86A, and R120A (Fig. 3A) and second-site mutations within VP1 for the remaining mutants except mutant K215A (Table 1). We then sequenced the whole genome of mutant K215A at P5, P10, and P20; however, no second-site mutations was found. These data together with the results of IFA and plaque assay (Fig. 2A and B) confirmed that the K215A mutation only delayed virus particle production.

**Verification of compensatory mutations.** To verify whether the second-site mutations listed in Table 1 are indeed responsible and sufficient to restore production of infectious particles, we introduced the second-site mutations into the infectious cDNA clone with the respective original mutations. IFA, virus production, and plaque morphology were compared between the WT and the reconstructed variants with second-site mutations in VP1 after the transfection of Vero cells with genome-length RNAs. As shown in Fig. 3B and C and Table 2, for the defective mutants R3A and R38A, the corresponding second-site mutations M63L and D40V fully restored the production of infectious particles. Double



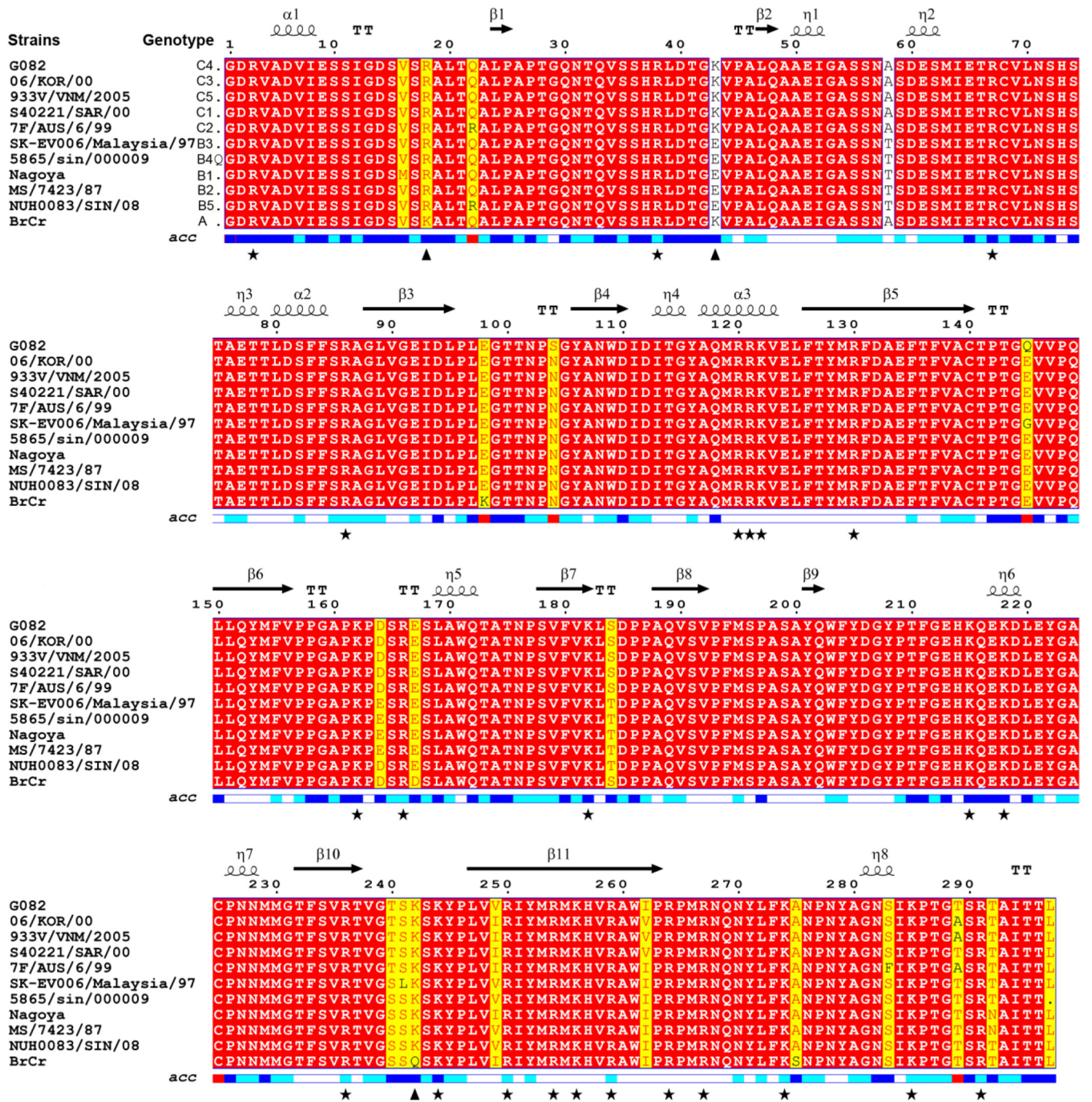


FIG 1 Amino acid sequence alignment of VP1 proteins from representative genotypes of EV71. The name of each EV71 strain from genotypes A, B1, B2, B3, B4, B5, C1, C2, C3, C4, and C5 is indicated on left. The numbering of amino acid sequences is based on strain G082 (genotype C4), which is used in this study. The secondary structure based on the EV71 structure model (Protein Data Bank code 3VBS) is shown above the sequence. Identical amino acids among all VP1 proteins are shown in red. The mutated positively charged residues in this study are indicated by triangles and asterisks below the sequence for nonconserved and completely conserved amino acids, respectively. The relative accessibility of each residue is shown at the bottom of the alignment: blue, accessible; cyan, intermediate; white, buried and red, not applicable. The figure was produced using ESPrnt.

mutants R3A+M63L and R38A+D40V produced amounts of infectious viruses similar to that for WT with no significant difference in plaque morphology. For defective mutant K242A, both second-site mutations E92G and T100K partially restored production of plaques and combined triple mutant K242A+E92G+T100K produced amounts of infectious viruses similar to that for WT, with

similar plaque morphology. For defective mutant K244A, second-site mutation T237N but not Q145K partially restored production of plaques and combined triple mutant K244A+Q145K+T237N slightly increased the infectivity of the double mutant K244A+T237N, which suggests that the Q145K mutation alone was not sufficient to restore the phenotype of the original revertants but

TABLE 1 Characterization of each mutation

Mutation	Location in VP1	Mean titer (PFU/ml) $\pm$ SD <sup>a</sup>	IFA <sup>b</sup>	Passage that displayed CPE <sup>c</sup>	Revertant <sup>d</sup>
WT		$(1.2 \pm 0.1) \times 10^6$	+++	P0	NA
R3A	N terminus	$(1.2 \pm 0.6) \times 10^{2*}$	+	P3	VP1 M63L
R18A	N terminus	$(1.4 \pm 0.4) \times 10^5$	+++	P0	NA
R38A	N terminus	$(1.2 \pm 1.0) \times 10^2$	++	P2	VP1 D40V
K43A	N terminus	$(1.8 \pm 0.2) \times 10^4$	++	P2	Reverted to WT
R67A	N terminus	ND	–	ND	ND
R86A	N terminus	$(5.3 \pm 2.5) \times 10^{2*}$	+	P2	Reverted to WT
R120A	$\alpha_3$	ND	–	P3	Reverted to WT
R121A	$\alpha_3$	ND	–	ND	ND
K122A	$\alpha_3$	ND	–	ND	ND
R130A	$\beta_{1D}$	ND	–	ND	ND
K162A	EF loop	$(1.5 \pm 0.2) \times 10^6$	+++	P0	NA
R166A	EF loop	ND	–	ND	ND
K182A	$\beta_F$	ND	–	ND	ND
K215A	GH loop	$(3.6 \pm 0.6) \times 10^{2*}$	–	P3	ND
K218A	GH loop	$(1.7 \pm 0.1) \times 10^6$	+++	P0	NA
R236A	$\beta_{1H}$	ND	–	ND	ND
K242A	HI loop	ND	–	P5	VP1 E92G, VP1 T100K
K244A	HI loop	ND	–	P8	VP1 Q145K, VP1 T237N
R250A	$\beta_1$	ND	–	P11	VP1 T41I, VP1 E167K
R254A	$\beta_1$	ND	–	ND	ND
K256A	$\beta_1$	ND	–	ND	ND
R259A	$\beta_1$	ND	–	ND	ND
R264A	C terminus	ND	–	ND	ND
R267A	C terminus	ND	–	ND	ND
K274A	C terminus	ND	–	P7	VP1 I111L, VP1 A224V
K285A	C terminus	$(2.0 \pm 0.8) \times 10^6$	+++	P0	NA
R291A	C terminus	ND	–	ND	ND

<sup>a</sup> The mean virus titers at 48 h p.t. were determined by plaque assay from three independent experiments. An asterisk represents the titer at 72 h p.t because the titer at 48 h.p.t was below the limit of detection. ND, not detected.

<sup>b</sup> For each mutant, IFA was repeated at least three times, and the positive rate was calculated from five random views under a microscope using Image-Pro Plus software. The positive rate for the WT was set as strong (+++) and mutant levels as strong (+++) (IFA positive rate  $\geq$ 66.7% of that of the WT), ++ (medium) (IFA positive rate between 33.3% and 66.7% of that of the WT), + (weak) (IFA positive rate between 5% and 33.3% of that of the WT), and negative (–) (IFA positive rate less than 5% of that of the WT).

<sup>c</sup> Defective mutants were subjected to revertant analysis by continuous culturing on Vero cells up to 20 rounds. CPE was monitored under a microscope. ND, the mutant did not display CPE by P20.

<sup>d</sup> NA, not applicable; ND, not detected.

had an additive effect on virus production. For lethal mutant R250A, second-site mutation E167K but not T41I was responsible for compensation and combined triple mutant R250A+T41I+E167K did not increase the virus production, and the viral titers of double mutant R250A+E167K and triple mutant R250A+T41I+E167K were much lower and the plaques were smaller than the WT. For lethal mutant K274A, second-site mutation I111L could compensate for the lethal effect of K274A, as to a lesser extent could mutation A224V, and combined triple mutant K274A+I111L+A224V showed virus production and plaque morphology similar to those for the WT. Only for mutant R250A, which displayed CPE at P11, were the second-site mutations in VP1 not sufficient to fully restore production of infectious particles; therefore, we sequenced the whole genome of P20, but no additional mutations were found (data not shown).

In addition, multistep growth curves for all the recombinant viruses containing the additional second-site mutations were determined, except for mutants R250A+E167K, R250A+T41I+E167K, and K274A+A224V which could not produce high-titer virus for infection at an MOI of 0.1. Consistent with the results of IFA and plaque assay, viral titers of all variants increased steadily with time by 72 h p.i., and all the tested mutants except mutants K242A+E92G, K244A+T237N, and K274A+I111L achieved

peak titers similar to that of the WT (Fig. 3D). Collectively, the data demonstrate that the identified second-site mutations are compensatory.

**Mutant K215A displays a higher thermal stability phenotype.** EV71 is a nonenveloped virus, and VP1 is the most surface-exposed capsid protein. To ask whether charged-to-alanine mutation in VP1 can affect the thermal stability of virus, we tested the thermal inactivation kinetics for all the mutants and revertants with titers higher than 10,000 PFU/ml. Wild-type virus and mutants were incubated at 42°C for different amounts of time, and their remaining infectivities were titrated by plaque assays. As shown in Fig. 4A, mutant K215A displayed a higher thermal stability phenotype than the WT, whereas other mutants showed stability similar to or lower than that of WT. After 2 h of treatment at 42°C, the relative remaining infectivity of mutant K215A was 32.6% higher than that of WT. These results indicated that the K215A mutation greatly improved virus thermostability. Residue K215 is located within the VP1 GH loop (Fig. 4B), which acts as an adaptor-sensor for cellular receptor attachment (14). The VP1 GH loop undergoes a major conformational switch during uncoating, and replacement of Lys by Ala at this position perhaps impairs the movement of the GH loop during protomer extension, resulting in a delay of conversion into an A-particle and



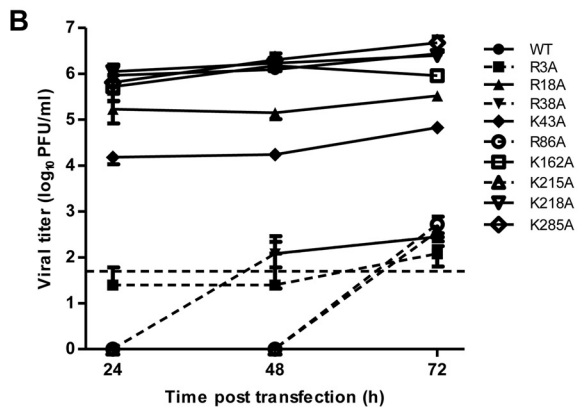
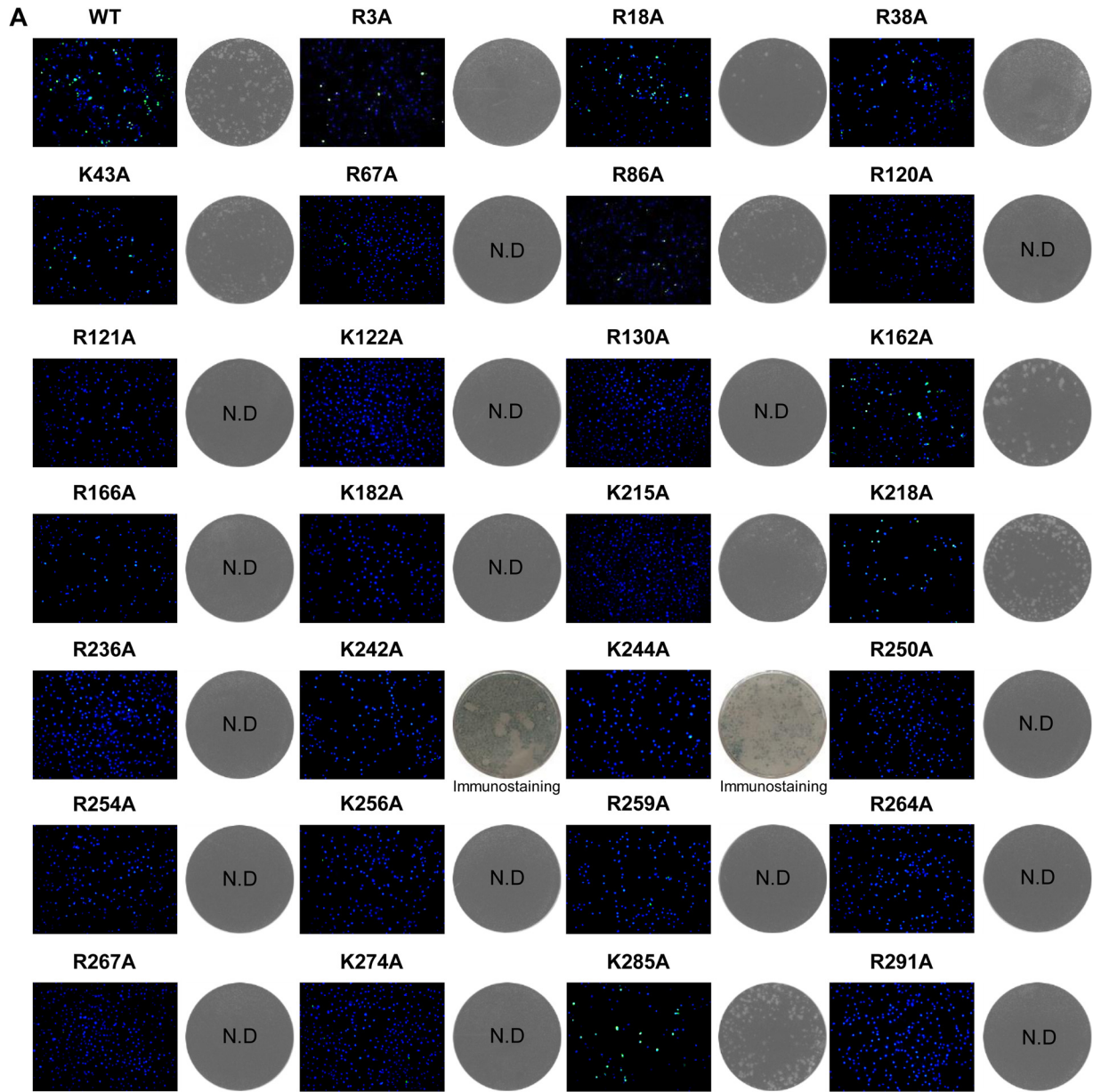


FIG 2 Analysis of EV71 VP1 charged-to-alanine scanning mutants. (A) Analysis of IFA and plaque morphology for each mutant. Vero cells were transfected with WT and mutant genome-length RNAs (10  $\mu$ g) and analyzed by IFA at 48 h posttransfection (left panels for each virus). For each IFA, anti-EV71 monoclonal antibody (MAB979) and goat anti-mouse IgG conjugated with Alexa Fluor 488 were used as primary and secondary antibodies, respectively. The cell nucleus was

subsequent release of the genome. Both heat treatment (e.g., at 56°C for 12 min) (23) and receptor binding could trigger a conformational change that opens up the capsid to form A-particles. Thus, the K215A mutation probably delays the process of conformational change triggered by receptor binding and heat treatment, which in turn slows the release of the genome, resulting in phenotypes of delayed virus production and higher thermal stability. Taking the findings together, conditional thermostable mutants can be generated by altering the charge characteristics of VP1. Rational engineering of viable EV71 virus with increased thermostability by introduction of a stabilizing mutation(s) using reverse genetic tools is an attractive approach for development of improved vaccines which reduce the dependence on a cold chain (36, 37).

**Sensitivities of mutants and revertants to an EV71 entry inhibitor.** EV71 uses cell surface heparan sulfate as an attachment receptor to initiate infection (21), and the negatively charged heparan sulfate moieties could nonspecifically interact with a region of positive charge in the capsid. We have recently identified suramin and sucralfate as EV71 entry inhibitors which could act as receptor mimetics, competing for EV71 virion binding to cellular heparan sulfate and thereby inhibiting EV71 infection (30, 32). In particular, suramin binds to the virus particle via the negatively charged naphthalenetrisulfonic acid group (30), which prompted us to test the hypothesis that the mutants containing positively charged-to-alanine mutations will become resistant to suramin inhibition. We then measured the sensitivities of mutant viruses to suramin in CPE assay. Surprisingly, all the mutants containing single charged-to-alanine mutations exhibited sensitivity to suramin, with less than a 1.1-fold shift in 50% effective concentrations ( $EC_{50}$ s) compared to that of the WT (Fig. 4C), and mutants K242A+E92G+T100K and K242A+T100K were slightly more sensitive to suramin inhibition, which suggests that single charged-to-alanine mutation is not sufficient for suramin resistance.

## DISCUSSION

The VP1 protein of EV71 plays a central role in the formation of infectious particles; however, the amino acids of the VP1 protein essential for this function are still undetermined. We sought to identify the amino acid residues of VP1 that are essential for production of infectious particles through alanine scanning mutagenesis. Our study showed that positively charged residues in EV71 VP1 are critical for this function, based on three lines of evidence: (i) most of positively charged residues (24 out of 27) are completely conserved among all the subgenogroups of EV71 (the exceptions are residues R18, K43, and K242); (ii) charged-to-alanine scanning analysis showed that 16 mutations are lethal and 7 mutations are defective; and (iii) 13 out of 23 defective or lethal mutants did not yield revertants even after 20 passages.

Given that positively charged residues in VP1 may provide electrostatic surface potential required for receptors binding or

genomic RNA interactions, the charged-to-alanine mutations could block receptor binding or disrupt packaging of viral RNA, leading to a defective or lethal phenotype. Unlike PSGL-1, which is expressed mainly on leukocytes, SCARB2 and heparan sulfate can be utilized by most EV71 strains as entry receptors. Chen et al. identified residue Q172 and surrounding residues in VP1 which form the canyon as the determinants of SCARB2 binding, and using a single-round pseudotype EV71 virus infection system, they showed that R166A and R236A mutations reduced SCARB2 binding and infection on RD cells but did not interfere with virus assembly (38). In agreement with their findings, we found that mutations R166A and R236A are lethal. Interestingly, residue R166 is also predicted to be the heparan sulfate binding site (21), with the overlap of receptor binding highlighting its functional role during initial attachment. Beside residue R166, residues K242 and K244 could also serve as the binding sites for heparan sulfate (21), and the defective phenotype of mutants K242A and K244A may be due to reduced heparan sulfate binding. Additionally, the crystal structure of the EV71 uncoating intermediate revealed that the N-terminal extensions of VP1 (residues 1 to 71) interact with the genomic RNA (35); therefore, the defective phenotype of mutants R3A, R38A, and K43A and the lethal phenotype of mutant R67A could be due to reduced or eliminated genomic RNA binding, although more experiments are necessary to prove this. Moreover, Lyu et al. recently reported that a hydrogen bonding network between the 5-fold-related residues K182 and D185 from a neighboring VP1 was maintained during uncoating (35). In our study, K182A was found to be a lethal mutation that presumably disrupts the network, highlighting the importance of maintaining the hydrogen bonding network.

The structures of the EV71 mature particle, empty particle, and uncoating intermediate provide meaningful information for this study. To understand how the second-site mutations may exert their compensatory effect, we looked at the structure of the EV71 mature particle (Protein Data Bank code 3VBS). For mutant R3A, an amino acid substitution of Met to Leu at position 63 (M63L) in the VP1 protein fully restored virus production. Leu is a hydrophobic residue with a slightly shorter side chain than Met, and the side chain of Leu has lower conformational flexibility and polarizability than that of Met. Thus, a relatively conservative substitution of Met to Leu will result in a more rigid capsid. Moreover, residue M63 is located far away from residue R3 on the same VP1 monomer (Fig. 5a, left), while it is close to residue R3 on the adjacent VP1 monomer of the pentamer (Fig. 5a, right), raising the possibility that alanine substitution at position 3 affects the transition of protomers into pentamers and that L63 on the neighboring VP1 monomer could compensate for this defect. For mutant R38A, an amino acid substitution of Asp to Val at position 40 (D40V) in the VP1 protein fully restored virus production. Residue D40 is proximate to R38 (Fig. 5b), and the electrostatic attraction between positively charged residue R38 and negatively charged residue D40 may stabilize the capsid during virus assem-

---

stained with DAPI (4',6-diamidino-2-phenylindole) and is presented in blue, the positive signal of EV71 is presented in green, and results from one representative experiment of three independent experiments is shown. Plaque morphologies of WT and mutant viruses are shown in the right panels for each virus. N.D., not detectable by either plaque assay or infectious center assay. (B) Virus release of EV71 mutants after transfection. Viruses from culture supernatants were collected every 24 h after transfection. Viral titers were determined by plaque assay on Vero cells. Error bars indicate the standard deviations from three independent experiments; the dashed line represents the limit of sensitivity of the plaque assay.

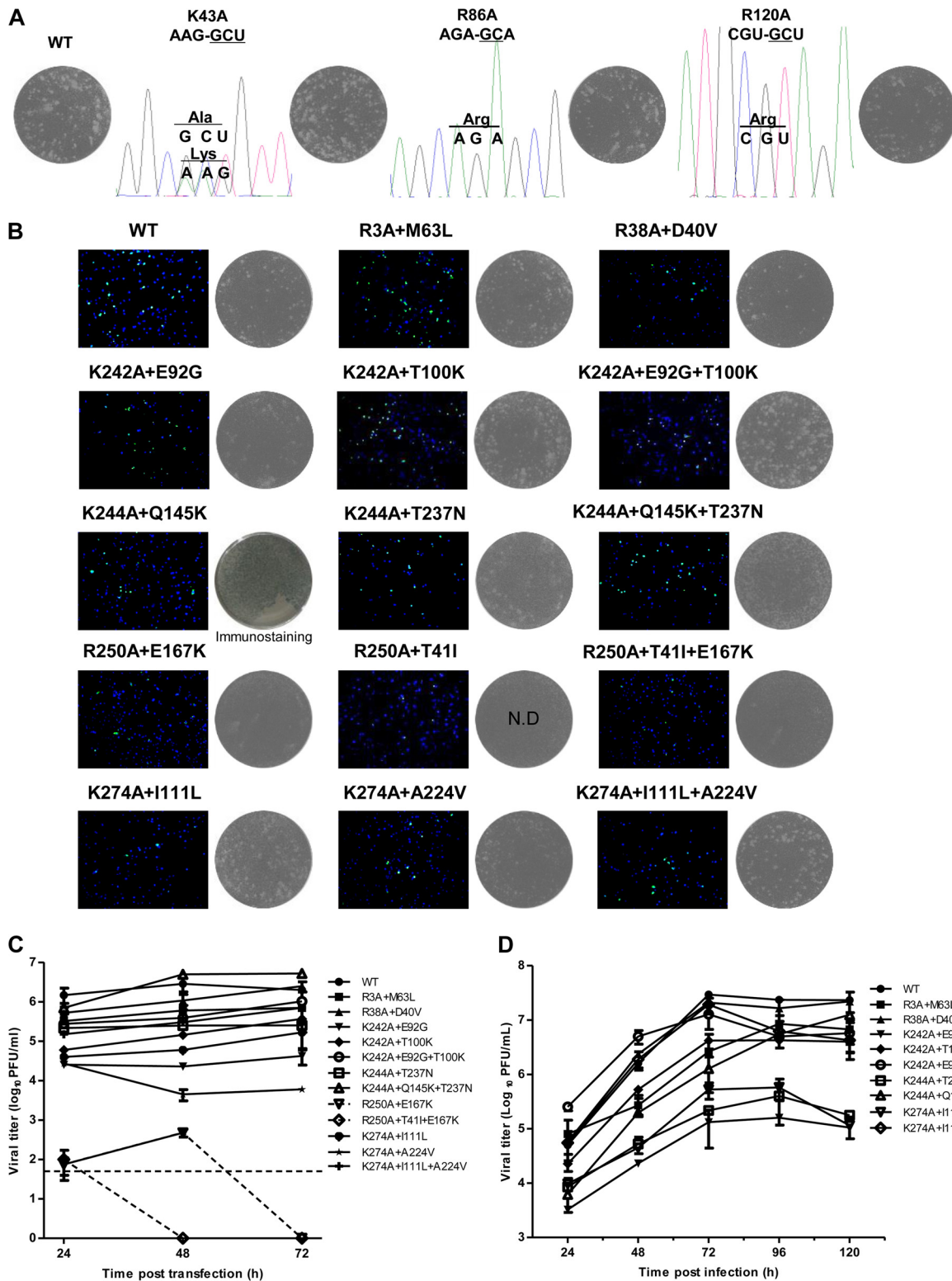


**FIG 3** Revertant analysis of EV71 charged-to-alanine scanning mutants. (A) The mutant viruses were continuously cultured on Vero cells for 20 rounds (P1 to P20). The plaque morphology and sequencing chromatogram for P5 are presented for the K43A, R86A, and R120A viruses, which revert to wild type. The engineered mutant nucleotides are underlined. (B) Verification of second-site mutations. *In vitro* transcripts of the indicated WT or mutant EV71 genomes containing combined mutations were transfected into Vero cells. IFA (left panels for each virus) and plaque assay were performed as described in the legend to Fig. 2A. Plaque morphologies of WT and mutant viruses are shown in the right panels for each virus. N.D., not detectable by either plaque assay or infectious center assay. (C) Production of VP1 mutant viruses after transfection. Supernatant was harvested at 24, 48, and 72 h p.t. and titrated on Vero cells. Error bars indicate the standard deviations from three independent experiments; the dashed line represents the limit of sensitivity of the plaque assay. (D) Growth kinetics of recombinant viruses containing compensatory mutations. Confluent Vero monolayers in 12-well plates were infected with the WT and mutant viruses containing compensatory mutations at an MOI of 0.1. After 1 h of incubation, the cells were washed three times with medium and replenished with 1 ml of medium. Viral titers in culture fluids were quantified at the indicated time points using plaque assays. The data shown were obtained from two independent replicates. Error bars indicate the standard deviations from two independent experiments.



TABLE 2 Characterization of recombinant viruses with secondary-site mutations

Recombinant virus	Mean titer (PFU/ml) $\pm$ SD <sup>a</sup>	IFA <sup>b</sup>
WT	$(2.9 \pm 1.1) \times 10^6$	+++
R3A+M63L	$(6.0 \pm 2.1) \times 10^5$	+++
R38A+D40V	$(1.1 \pm 0.5) \times 10^6$	+++
K242A+E92G	$(2.3 \pm 0.07) \times 10^4$	++
K242A+T100K	$(1.5 \pm 0.2) \times 10^5$	+++
K242A+E92G+T100K	$(3.9 \pm 0.4) \times 10^5$	+++
K244A+Q145K	ND	+
K244A+T237N	$(2.5 \pm 0.4) \times 10^5$	+++
K244A+Q145K+T237N	$(5.0 \pm 0.7) \times 10^6$	+++
R250A+T41I	ND	+
R250A+E167K	$(4.8 \pm 1.1) \times 10^2$	+
R250A+T41I+E167K	100 $\pm$ 70*	+
K274A+I111L	$(6.0 \pm 0.7) \times 10^4$	++
K274A+A224V	$(4.5 \pm 1.4) \times 10^3$	++
K274A+I111L+A224V	$(3.0 \pm 0.3) \times 10^5$	+++

<sup>a</sup> The mean virus titers at 48 h p.t. were determined by plaque assay from three independent experiments. An asterisk represents the virus titer at 24 h p.t. because the titers at 48 h p.t. and 72 h p.t. were below the limit of detection. ND, not detected.

<sup>b</sup> IFA was repeated at least three times, and the positive rate was calculated from five random views under a microscope using Image-Pro Plus software. The positive rate for the WT was set as strong (+++) and mutant levels as strong (+++) (IFA positive rate  $\geq$  66.7% of that of the WT), ++ (medium) (IFA positive rate between 33.3% and 66.7% of that of the WT), + (weak) (IFA positive rate between 5% and 33.3% of that of the WT), and negative (-) (IFA positive rate less than 5% of that of the WT).

bly and/or entry/uncoating. According to our multiple-sequence alignment results for the VP1 protein (Fig. 1), residues R38 and D40 are completely conserved among all EV71 genotypes, suggesting that the two residues of all EV71 viruses may interact with each other via electrostatic attractive force, thus facilitating virus production. When residue R38 is mutated to Ala, a negative to neutral change at position 40 (D40V) will balance the electrostatic surface potential, thereby restoring virus production. Along the same line, a negative to neutral change at position 92 (E92G) or a neutral to positive change at position 100 (T100K) probably alleviates electrostatic interference caused by the change of Lys to Ala at position 242 (Fig. 5c), thereby rescuing the defect of the K242A mutation. For mutant K244A, the Q145K mutation had an additive effect on virus production, residue VP1-145 has been reported to act as a switch controlling PSGL-1 binding by modulating the exposure of VP1-244K, VP1-145 in the DE loop makes close contact with residue VP1-244 in the HI loop from an adjacent protomer (25) (Fig. 5d), and when Q is at VP1-145, the side chain of residue K244 projects outward with the positively charged amino group exposed on the virus surface, leading to PSGL-1 binding. However, no PSGL-1 could be detected on the Vero cell surface (22); therefore, the defect of the K244A mutation observed on Vero cells is not due to the abolished PSGL-1 binding. The T237N mutation located in the  $\beta_{II}$  barrel rescued the defect of the K244A mutation, and the identical mutation was found in a recombinant EV71 virus (strain Nagoya) containing residues VP1 E98+G145 (25). Taking these together with our findings, we propose an interaction model of residues VP1-145, -244, and -237 in which residue VP1-244 interacts with residue VP1-237 on the same monomer and residue VP1-145 on the adjacent monomer. Besides, residues R166, K242, and K244 were clustered symmetrically at the 5-fold axis of the pentamer and exposed on the surfaces

of virus particles and thus were predicted to be heparan sulfate binding sites (21). Replacement of these positively charged residues by alanine would reduce the heparan sulfate binding, leading to a defective (mutants K242A and K244A) or lethal (mutant R166A) phenotype; therefore, another possibility for compensatory mutations E92G and T100K for mutant K242A and Q145K for mutant K244A is that they enhanced the heparan sulfate binding by increasing positive electrostatic potential. For mutant R250A, a second nonconservative mutation, E167K (Fig. 1), rescued the lethal phenotype of the R250A mutation. Residue E167 in the EF loop is positioned against positively charged residue R250 on the adjacent monomer (Fig. 5e), and when Arg at the position 250 was mutated to Ala, the electrostatic attraction between residue R250 and E167 was disrupted. A replacement of Glu with Lys at position 167 increased the positive electrostatic potential, which may restore their interactions between VP1 monomers, thereby stabilizing the capsid assembly. Interestingly, mutation E167G or E167A was found to be frequently associated with the VP1 L97R mutation, which conferred increased neural cell tropism during human EV71 infection (24), suggesting that residue E167 plays a central role in capsid assembly through interaction with residues L97 and R250. For mutant K274A, both mutations I111L and A224V could rescue the lethal phenotype of the K274A mutation. All these residues are close to sphingosine (Fig. 5f), the pocket factor that plays an essential role in regulating particle stability (39, 40). The side chain of Ala is much shorter than that of Lys, and thus a change of Lys to Ala at position 274 would increase the volume of the hydrophobic pocket, leading to destabilization of the capsid. Residue I111 is involved in the formation of the VP1 hydrophobic pocket (14), and residue A224 is close to the pocket factor; therefore changes of Ile to Leu at position 111 and Ala to Val at position 224 would constrain the volume of hydrophobic pocket with their larger side chains, which in turn stabilize the capsid and rescue the lethal phenotype of the K274A mutation.

Since VP1 is the most surface-exposed structural protein in EV71, charged-to-alanine mutations in this region may result in a change in thermal stability or resistance to an entry inhibitor which binds to virus particle via the negatively charged chemical group. Our observation that mutant K215A is more thermostable suggests that it possesses a more stable capsid. Wang et al. proposed an enterovirus uncoating model from structures of EV71 in which the VP1 GH loop acts as an adaptor-sensor (14), and the movement of the VP1 GH loop causes the conformational change during uncoating. Residues K215 and K218 are located within the VP1 GH loop; however, only mutant K215A displayed higher thermal stability and slower virus production than the WT, suggesting that a specific site(s) in the VP1 GH loop is important for sensing the heat treatment and receptor binding. A thermostable live attenuated enterovirus would be an ideal vaccine candidate, and our study indicated that the VP1 GH loop of enterovirus could be a promising target for rational vaccine design. Notably, none of the tested mutants was resistant to suramin, suggesting that single charged-to-alanine mutation is not sufficient for suramin resistance.

It should be noted that all the residues discussed in this study are still possibly involved in other aspects of the virus life cycle. By selecting revertants, we identified compensatory second-site mutations for four defective and two lethal mutants which suggest that intra- and intermolecular interactions of VP1 protein are vital

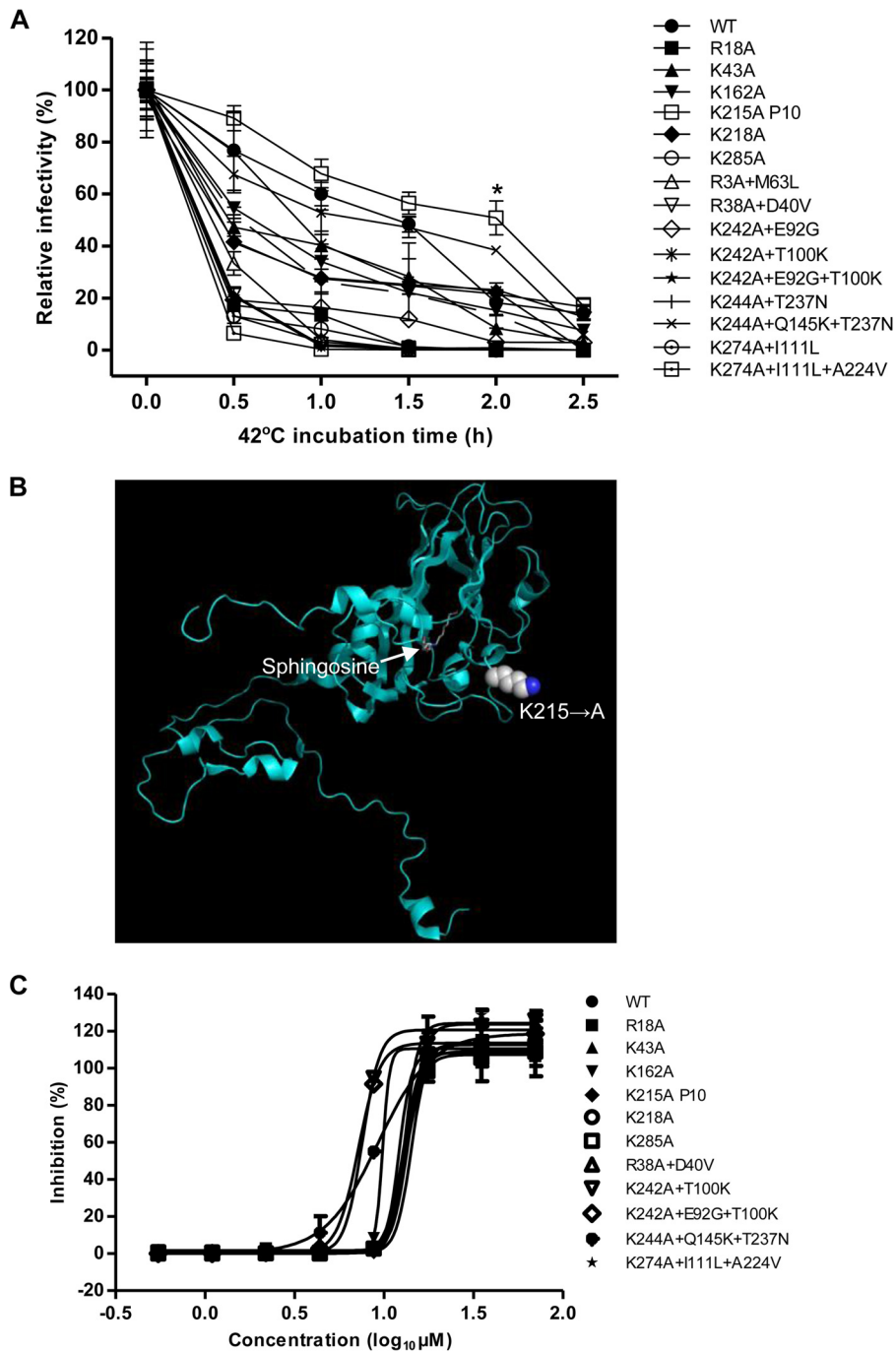


**FIG 4** Thermal inactivation kinetics at 42°C and sensitivity to suramin of some EV71 mutants. (A) Thermal stability analysis of EV71 mutant viruses at 42°C. The relative remaining infectivity is presented on a percent scale as a function of incubation time. Average results from two experiments are shown. Error bars represent the standard deviations from two independent experiments. Differences between the WT and mutants were compared using an unpaired, two-tailed Student *t* test (\*,  $P < 0.05$ ). (B) Localization of residue K215 on VP1, where Lys is mutated to Ala. The VP1 structure (PDB 3VBS) is shown in cyan; the pocket factor sphingosine is also indicated. (C) Suramin resistance analyses of mutant viruses in CPE assay. Twofold serially diluted suramin was added to Vero cells, and the inhibitory effects of the compound were analyzed by CPE assay (see details in Materials and Methods). The data presented were obtained from two independent experiments. Error bars represent the standard deviations from two independent measurements.

to virus production. The results provide important clues as to how these interactions between specific residues of VP1 in the same or an adjacent monomer regulate virus assembly and/or entry/uncoating. Whether a similar interaction also applies to other enteroviruses needs further investigation. Inhibiting these interac-

tions is a potential strategy for blocking EV71 particle production. Overall, our findings will broaden our understanding of EV71 assembly and entry. This knowledge will also be useful for the development of new vaccines and antivirals against EV71. It will be of interest to see whether the results for EV71 can be applied to

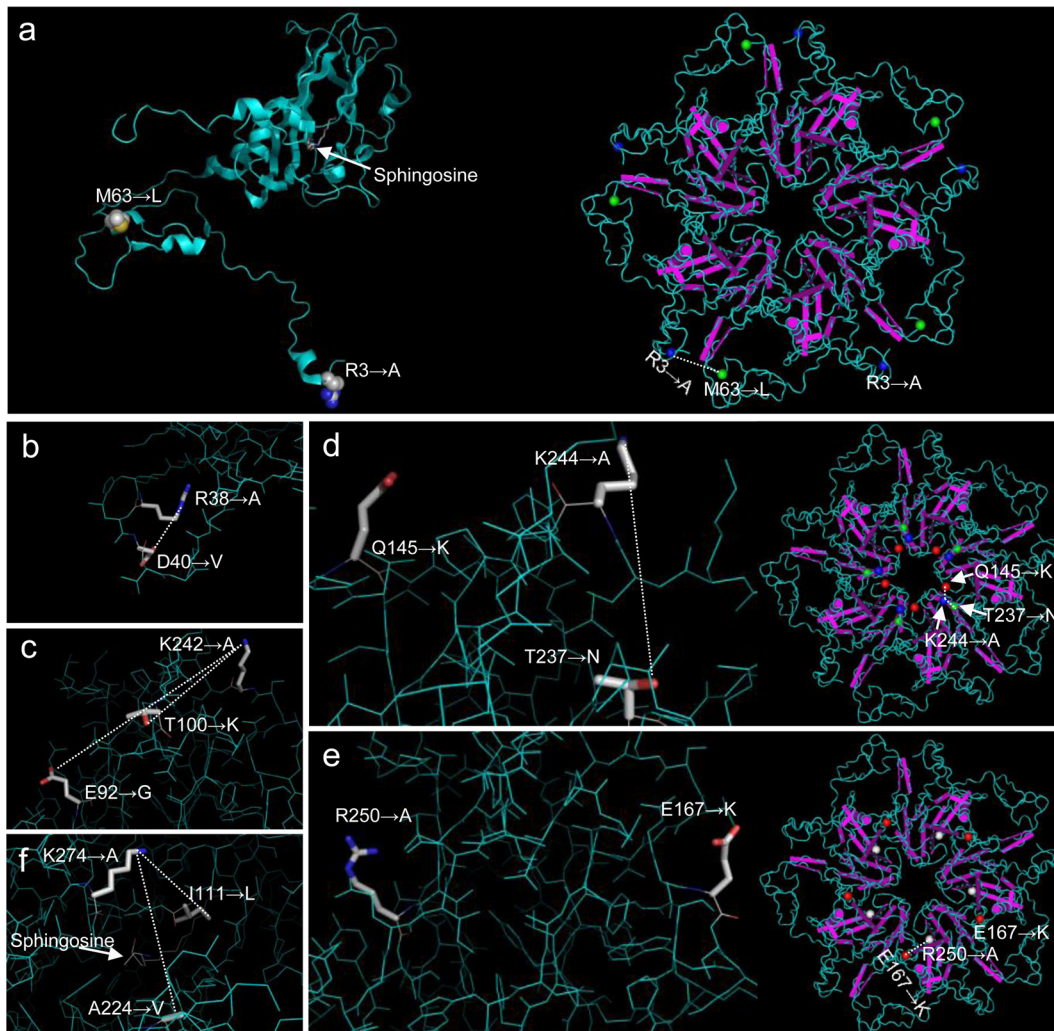


**FIG 5** Locations of mutants with second-site compensatory mutations in the structure model of EV71 VP1 (PDB 3VBS). The VP1 structure is shown in cyan, and for each side chain and the pocket factor sphingosine, elements are shown as follows: C, white; H, gray; N, blue; O, red; and S, orange. (a) Localization on a capsid protomer (left panel) and pentamer (right panel) of residues 3 (blue), where Arg was mutated to Ala, and 63 (green), where a second-site mutation from Met to Leu fully restored virus production. (b) Asp40 was mutated to Val to restore the infectivity of mutant R38A. (c) Glu92 and Thr100 were mutated to Gly and Lys, respectively, to restore the infectivity of mutant K242A. (d) Gln145 and Thr237 were mutated to Lys and Asn, respectively, to restore the infectivity of mutant K244A. The locations of residues Lys244 (blue), Gln145 (red), and Thr237 (green) are shown either on a VP1 monomer (left panel) or pentamer (right panel). (e) Localization on a capsid protomer (left panel) and pentamer (right panel) of residues 250 (white), where a lethal mutation from Arg to Ala was introduced, and 167 (red), where a second-site mutation from Glu to Lys partially restored virus production. (f) Localization on a capsid protomer of residue K274 and second-site mutation I111L and A224V, which partially restored the infectivity of lethal mutant K274A. This figure was produced using PyMol and Cn3D for protomer and pentamer, respectively.

other members of the *Enterovirus* genus or to other genera within the *Picornaviridae* family.

#### ACKNOWLEDGMENTS

We thank all the lab members for technical support and helpful discussions during the study.

This research was partially supported by funding from the National Natural Science Foundation of China (grant no. 31270204 and 31400148), the Science and Technology Commission of Shanghai Municipality (grant no. 14YF1407600), and the CAS-SIBS Frontier Research Field Foundation for Young Scientists (grant no. 2014KIP109). G.Z. gratefully acknowledges the support of the SA-SIBS scholarship program.

#### FUNDING INFORMATION

CAS-SIBS Frontier Research Foundation provided funding to Gang ZOU under grant number 2014KIP109. National Natural Science Foundation of China (NSFC) provided funding to Ralf Altmeyer under grant number 31270204. National Natural Science Foundation of China (NSFC) provided funding to Gang ZOU under grant number 31400148. Science and Technology Commission of Shanghai Municipality (STCSM) provided funding to Gang ZOU under grant number 14YF1407600.

#### REFERENCES

- Schmidt NJ, Lennette EH, Ho HH. 1974. An apparently new enterovirus isolated from patients with disease of the central nervous system. *J Infect Dis* 129:304–309. <http://dx.doi.org/10.1093/infdis/129.3.304>.
- Xing W, Liao Q, Viboud C, Zhang J, Sun J, Wu JT, Chang Z, Liu F,



- Fang VJ, Zheng Y, Cowling BJ, Varma JK, Farrar JJ, Leung GM, Yu H. 2014. Hand, foot, and mouth disease in China, 2008–12: an epidemiological study. *Lancet Infect Dis* 14:308–318. [http://dx.doi.org/10.1016/S1473-3099\(13\)70342-6](http://dx.doi.org/10.1016/S1473-3099(13)70342-6).
3. Ho M, Chen ER, Hsu KH, Twu SJ, Chen KT, Tsai SF, Wang JR, Shih SR. 1999. An epidemic of enterovirus 71 infection in Taiwan. Taiwan Enterovirus Epidemic Working Group. *N Engl J Med* 341:929–935.
  4. Chan KP, Goh KT, Chong CY, Teo ES, Lau G, Ling AE. 2003. Epidemic hand, foot and mouth disease caused by human enterovirus 71, Singapore. *Emerg Infect Dis* 9:78–85. <http://dx.doi.org/10.3201/eid1301.020112>.
  5. Tu PV, Thao NT, Perera D, Huu TK, Tien NT, Thuong TC, How OM, Cardosa MJ, McMinn PC. 2007. Epidemiologic and virologic investigation of hand, foot, and mouth disease, southern Vietnam, 2005. *Emerg Infect Dis* 13:1733–1741. <http://dx.doi.org/10.3201/eid1311.070632>.
  6. Zhang Y, Zhu Z, Yang W, Ren J, Tan X, Wang Y, Mao N, Xu S, Zhu S, Cui A, Yan D, Li Q, Dong X, Zhang J, Zhao Y, Wan J, Feng Z, Sun J, Wang S, Li D, Xu W. 2010. An emerging recombinant human enterovirus 71 responsible for the 2008 outbreak of hand foot and mouth disease in Fuyang city of China. *Virology* 7:94. <http://dx.doi.org/10.1186/1743-422X-7-94>.
  7. Seiff A. 2012. Cambodia unravels cause of mystery illness. *Lancet* 380:206. [http://dx.doi.org/10.1016/S0140-6736\(12\)61201-X](http://dx.doi.org/10.1016/S0140-6736(12)61201-X).
  8. Kung YA, Hung CT, Liu YC, Shih SR. 2014. Update on the development of enterovirus 71 vaccines. *Expert Opin Biol Ther* 14:1455–1464. <http://dx.doi.org/10.1517/14712598.2014.935330>.
  9. Wimmer E, Hellen CU, Cao X. 1993. Genetics of poliovirus. *Annu Rev Genet* 27:353–436. <http://dx.doi.org/10.1146/annurev.ge.27.120193.002033>.
  10. Racaniello V. 2006. Picornaviridae: the viruses and their replication, p 796–838. *In* Knipe D, Howley P (ed), *Fields virology*, 5th ed. Lippincott Williams & Wilkins, Philadelphia, PA.
  11. Tuthill TJ, Groppelli E, Hogle JM, Rowlands DJ. 2010. Picornaviruses. *Curr Top Microbiol Immunol* 343:43–89. [http://dx.doi.org/10.1007/82\\_2010\\_37.20397067](http://dx.doi.org/10.1007/82_2010_37.20397067).
  12. Curry S, Fry E, Blakemore W, Abu-Ghazaleh R, Jackson T, King A, Lea S, Newman J, Stuart D. 1997. Dissecting the roles of VP0 cleavage and RNA packaging in picornavirus capsid stabilization: the structure of empty capsids of foot-and-mouth disease virus. *J Virol* 71:9743–9752.
  13. Basavappa R, Syed R, Flore O, Icenogle JP, Filman DJ, Hogle JM. 1994. Role and mechanism of the maturation cleavage of VP0 in poliovirus assembly: structure of the empty capsid assembly intermediate at 2.9 Å resolution. *Protein Sci* 3:1651–1669. <http://dx.doi.org/10.1002/pro.5560031005>.
  14. Wang X, Peng W, Ren J, Hu Z, Xu J, Lou Z, Li X, Yin W, Shen X, Porta C, Walter TS, Evans G, Axford D, Owen R, Rowlands DJ, Wang J, Stuart DJ, Fry EE, Rao Z. 2012. A sensor-adaptor mechanism for enterovirus uncoating from structures of EV71. *Nat Struct Mol Biol* 19:424–429. <http://dx.doi.org/10.1038/nsmb.2255>.
  15. Plevka P, Perera R, Cardosa J, Kuhn RJ, Rossmann MG. 2012. Crystal structure of human enterovirus 71. *Science* 336:1274. <http://dx.doi.org/10.1126/science.1218713>.
  16. Nishimura Y, Shimojima M, Tano Y, Miyamura T, Wakita T, Shimizu H. 2009. Human P-selectin glycoprotein ligand-1 is a functional receptor for enterovirus 71. *Nat Med* 15:794–797. <http://dx.doi.org/10.1038/nm.1961>.
  17. Yamayoshi S, Yamashita Y, Li J, Hanagata N, Minowa T, Takemura T, Koike S. 2009. Scavenger receptor B2 is a cellular receptor for enterovirus 71. *Nat Med* 15:798–801. <http://dx.doi.org/10.1038/nm.1992>.
  18. Yang B, Chuang H, Yang KD. 2009. Sialylated glycans as receptor and inhibitor of enterovirus 71 infection to DLD-1 intestinal cells. *Virology* 6:141. <http://dx.doi.org/10.1186/1743-422X-6-141>.
  19. Su PY, Liu YT, Chang HY, Huang SW, Wang YF, Yu CK, Wang JR, Chang CF. 2012. Cell surface sialylation affects binding of enterovirus 71 to rhabdomyosarcoma and neuroblastoma cells. *BMC Microbiol* 12:162. <http://dx.doi.org/10.1186/1471-2180-12-162>.
  20. Yang SL, Chou YT, Wu CN, Ho MS. 2011. Annexin II binds to capsid protein VP1 of enterovirus 71 and enhances viral infectivity. *J Virol* 85:11809–11820. <http://dx.doi.org/10.1128/JVI.00297-11>.
  21. Tan CW, Poh CL, Sam IC, Chan YF. 2013. Enterovirus 71 uses cell surface heparan sulfate glycosaminoglycan as an attachment receptor. *J Virol* 87:611–620. <http://dx.doi.org/10.1128/JVI.02226-12>.
  22. Du N, Cong H, Tian H, Zhang H, Zhang W, Song L, Tien P. 2014. Cell surface vimentin is an attachment receptor for enterovirus 71. *J Virol* 88:5816–5833. <http://dx.doi.org/10.1128/JVI.03826-13>.
  23. Shingler KL, Yoder JL, Carnegie MS, Ashley RE, Makhov AM, Conway JF, Hafenstein S. 2013. The enterovirus 71 A-particle forms a gateway to allow genome release: a cryoEM study of picornavirus uncoating. *PLoS Pathog* 9:e1003240. <http://dx.doi.org/10.1371/journal.ppat.1003240>.
  24. Cordey S, Petty TJ, Schibler M, Martinez Y, Gerlach D, van Belle S, Turin L, Zdobnov E, Kaiser L, Tapparel C. 2012. Identification of site-specific adaptations conferring increased neural cell tropism during human enterovirus 71 infection. *PLoS Pathog* 8:e1002826. <http://dx.doi.org/10.1371/journal.ppat.1002826>.
  25. Nishimura Y, Lee H, Hafenstein S, Kataoka C, Wakita T, Bergelson JM, Shimizu H. 2013. Enterovirus 71 binding to PSGL-1 on leukocytes: VP1-145 acts as a molecular switch to control receptor interaction. *PLoS Pathog* 9:e1003511. <http://dx.doi.org/10.1371/journal.ppat.1003511>.
  26. Chang SC, Li WC, Chen GW, Tsao KC, Huang CG, Huang YC, Chiu CH, Kuo CY, Tsai KN, Shih SR, Lin TY. 2012. Genetic characterization of enterovirus 71 isolated from patients with severe disease by comparative analysis of complete genomes. *J Med Virol* 84:931–939. <http://dx.doi.org/10.1002/jmv.23287>.
  27. Li R, Zou Q, Chen L, Zhang H, Wang Y. 2011. Molecular analysis of virulent determinants of enterovirus 71. *PLoS One* 6:e26237. <http://dx.doi.org/10.1371/journal.pone.0026237>.
  28. Shih SR, Tsai MC, Tseng SN, Won KF, Shia KS, Li WT, Chern JH, Chen GW, Lee CC, Lee YC, Peng KC, Chao YS. 2004. Mutation in enterovirus 71 capsid protein VP1 confers resistance to the inhibitory effects of pyridyl imidazolidinone. *Antimicrob Agents Chemother* 48:3523–3529. <http://dx.doi.org/10.1128/AAC.48.9.3523-3529.2004>.
  29. Arita M, Wakita T, Shimizu H. 2008. Characterization of pharmacologically active compounds that inhibit poliovirus and enterovirus 71 infectivity. *J Gen Virol* 89:2518–2530. <http://dx.doi.org/10.1099/vir.0.2008/002915-0>.
  30. Ren P, Zou G, Bailly B, Xu S, Zeng M, Chen X, Sheng L, Zhang Y, Guillon P, Arenzana-Seisdedos F, Buchy P, Li J, von Itzstein M, Li Q, Altmeyer R. 2014. The approved pediatric drug suramin identified as a clinical candidate for the treatment of EV71 infection—suramin inhibits EV71 infection in vitro & in vivo. *Emerg Microbes Infect* 3:e62. <http://dx.doi.org/10.1038/emi.2014.60>.
  31. Wang Y, Qing J, Sun Y, Rao Z. 2014. Suramin inhibits EV71 infection. *Antiviral Res* 103:1–6. <http://dx.doi.org/10.1016/j.antiviral.2013.12.008>.
  32. Gao Q, Yuan S, Zhang C, Wang Y, Wang Y, He G, Zhang S, Altmeyer R, Zou G. 2015. Discovery of itraconazole with broad-spectrum in vitro antienterovirus activity that targets nonstructural protein 3A. *Antimicrob Agents Chemother* 59:2654–2665. <http://dx.doi.org/10.1128/AAC.05108-14>.
  33. Zou G, Zhang B, Lim PY, Yuan Z, Bernard KA, Shi PY. 2009. Exclusion of West Nile virus superinfection through RNA replication. *J Virol* 83:11765–11776. <http://dx.doi.org/10.1128/JVI.01205-09>.
  34. Chan YF, Sam IC, AbuBakar S. 2010. Phylogenetic designation of enterovirus 71 genotypes and subgenotypes using complete genome sequences. *Infect Genet Evol* 10:404–412. <http://dx.doi.org/10.1016/j.meegid.2009.05.010>.
  35. Lyu K, Ding J, Han JF, Zhang Y, Wu XY, He YL, Qin CF, Chen R. 2014. Human enterovirus 71 uncoating captured at atomic resolution. *J Virol* 88:3114–3126. <http://dx.doi.org/10.1128/JVI.03029-13>.
  36. Mateo R, Luna E, Rincon V, Mateo MG. 2008. Engineering viable foot-and-mouth disease viruses with increased thermostability as a step in the development of improved vaccines. *J Virol* 82:12232–12240. <http://dx.doi.org/10.1128/JVI.01553-08>.
  37. Wang G, Cao RY, Chen R, Mo L, Han JF, Wang X, Xu X, Jiang T, Deng YQ, Lyu K, Zhu SY, Qin ED, Tang R, Qin CF. 2013. Rational design of thermostable vaccines by engineered peptide-induced virus self-biomimetalization under physiological conditions. *Proc Natl Acad Sci U S A* 110:7619–7624. <http://dx.doi.org/10.1073/pnas.1300233110>.
  38. Chen P, Song Z, Qi Y, Feng X, Xu N, Sun Y, Wu X, Yao X, Mao Q, Li X, Dong W, Wan X, Huang N, Shen X, Liang Z, Li W. 2012. Molecular determinants of enterovirus 71 viral entry: cleft around GLN-172 on VP1 protein interacts with variable region on scavenger receptor B 2. *J Biol Chem* 287:6406–6420. <http://dx.doi.org/10.1074/jbc.M111.301622>.
  39. Rossmann MG. 1994. Viral cell recognition and entry. *Protein Sci* 3:1712–1725. <http://dx.doi.org/10.1002/pro.5560031010>.
  40. Rossmann MG, He Y, Kuhn RJ. 2002. Picornavirus-receptor interactions. *Trends Microbiol* 10:324–331. [http://dx.doi.org/10.1016/S0966-842X\(02\)02383-1](http://dx.doi.org/10.1016/S0966-842X(02)02383-1).